Measurements of ordinary muon capture rates on ^{100}Mo and natural Mo for astro-antineutrinos and double-β decays

I. H. Hashim [ORCID],[*] N. N. A. M. A. Ghani, F. Othman, R. Razali [ORCID], and Z. W. Ng [ORCID]

Department of Physics, Faculty of Science, Universiti Teknologi Malaysia, 81310 Johor Bahru, Johor, Malaysia

H. Ejiri [ORCID], T. Shima, and D. Tomono

Research Centre for Nuclear Physics, 10-1 Mihogaoka, Ibaraki, Osaka 567-0047, Japan

D. Zinatulina, M. Schirchenko [ORCID], and S. Kazartsev [ORCID]

Joint Institute for Nuclear Research, 6 Joliot-Curie St, 141980 Dubna, Moscow Region, Russia

A. Sato [ORCID] and Y. Kawashima

Department of Physics, Graduate School of Science, Osaka University, Machikaneyama 1-1, Toyonaka, Osaka 564-0043, Japan

K. Ninomiya

Department of Chemistry, Graduate School of Science, Osaka University, Machikaneyama 1-1, Toyonaka, Osaka 564-0043, Japan

K. Takahisa

Department of Radiological Technology, Faculty of Health Sciences, Kobe Tokiwa University,
Otani 2-6-2, Nagata, Kobe, Hyogo 653-0838, Japan

Ordinary muon capture (OMC) rates are valuable for studying the neutrino nuclear responses of astrophysical antineutrinos and double-β decays (DBDs). Currently, there is interest in experimental studies of the OMC rates and their mass number (A) dependence for ^{100}Mo and natural Mo. To obtain these rates, a negative muon beam from the MuSIC facility at the Research Center for Nuclear Physics (RCNP), Osaka University was utilized. The half-lives of trapped muons were measured by using a muon stopping signal from a scintillation counter and the time distribution of the OMC nuclear gamma rays and the muon-decay electrons by Ge detectors. The present measurements yielded OMC rates for enriched and natural molybdenum of $\Lambda(^{100}\text{Mo}) = (7.07 \pm 0.32) \times 10^6 \text{ s}^{-1}$ and $\Lambda(^{\text{nat}}\text{Mo}) = (9.66 \pm 0.44) \times 10^6 \text{ s}^{-1}$, respectively. The observed OMC rate for ^{100}Mo is approximately 27% smaller than that for natural Mo due to the blocking effect of the excess neutrons on the proton-to-neutron transformation in OMC. The present experimental observation is consistent with the Goulard-Primakoff (GP) and Primakoff (P) empirical equations. The impacts of the present results on the astro-antineutrinos and double-β decays are discussed.

I. INTRODUCTION

Neutrinoless double-β ($0\nu\beta\beta$) decays and supernova neutrinos are currently of interest for studying neutrinos beyond and within the standard model. They play a crucial role in investigating neutrino properties and weak interactions that go beyond the electroweak standard theory. Additionally, they contribute to the understanding of supernova neutrino/antineutrino nuclear syntheses and nuclear interactions, as discussed in the review papers by Ejiri *et al.* [1–4] and references therein.

To determine the rates of $0\nu\beta\beta$ decay ($R^{0\nu}$), it is necessary to calculate the coherent sum of the individual matrix elements ($M_i^{0\nu}$) [5]. In the investigation of each intermediate state (i), researchers are currently exploring two corresponding isospin $\tau^{\pm}$ directions using nuclear, lepton, and photon probes [1,6]. The τ^{+} operator represents the proton-to-neutron transition, acting as the isospin raising operator. On the other hand, the τ^{-} operator represents the neutron-to-proton transition and functions as the isospin lowering operator [1].

The neutrino responses for τ^{-} have been investigated through charge exchange reactions (CER) using $(^3\text{He}, t)$ to evaluate the single β^{-} matrix, $M(\beta^{-})$ [7,8]. On the other hand, the τ^{+} responses are studied through ordinary muon capture (OMC) reactions and photonuclear reactions via isobaric analog states (IAS) [1,3].

OMC is a weak nuclear process involving the exchange of a charged weak boson, where a negative muon is captured

on a medium-heavy nucleus $^A_Z X$, resulting in a highly excited compound nucleus of $^A_{Z-1} Y$ with an excitation energy of up to 100 MeV, equivalent to the mass of the muon [5]. Subsequently, a muon neutrino is emitted, carrying an energy of approximately 100–50 MeV [5]. The residual nucleus $^A_{Z-1} Y$ after OMC remains in the excitation energy range of $E = 0$–50 MeV and momentum transfer of 100–50 MeV/c [5], similar to double-β decays (DBDs) and supernova neutrino interactions.

The τ^+ responses in medium-heavy nuclei involving proton (p) to neutron (n) transformations are sensitive to the neutron excess caused by the generation of additional neutrons. It is worth noting that most DBDs are studied using isotopes with the highest $N - Z$. Experimental studies demonstrate that the OMC rate decreases with increasing mass number (A) [9–14]. Nuclei with larger N exhibit significantly lower OMC rates due to the blocking effect of low-energy p-to-n transitions caused by the excess neutrons in the nuclei. However, a significant increase in the OMC rate is observed when the second and higher forbidden transitions are involved [12].

The present study aims to investigate the OMC rates for ^{100}Mo and ^{nat}Mo in order to examine the $N - Z$ dependence of OMC in Mo isotopes, which are of interest for astro-antineutrinos [4] and DBDs [1]. The OMC rate associated with the τ^+ response, denoted as Λ^{cap}_μ, can be directly evaluated through the muon disappearance rate by observing the electrons resulting from the weak decays of the bound negative muons in the nucleus as a function of time [11,14]. The total muon disappearance rate Λ^{total}_μ is given by

$$\Lambda^{total}_\mu = \frac{1}{\tau_\mu} = \Lambda^{cap}_\mu + H \times \Lambda_{decay} \tag{1}$$

where Λ^{cap}_μ indicates the OMC rate, H is the Huff factor, and the free muon decay rate is given by $\Lambda_{decay} = (0.455 \pm 0.005) \times 10^6$ s^{-1}. The Huff factor represents the overlap of the muon and electron wave functions compared to that in free muon decay. It takes into account the combined effects of phase space, time dilation, and the Coulomb force on the decay products [15]. The decay rate of the free muon is derived from the inverse average muon lifetime, τ_μ [9,16].

The review article by Measday [14] provides a detailed discussion of the OMC rates. Additionally, a proton-neutron emission model (PNEM) has been developed to examine the overall distribution of final states following the OMC reaction, as well as the branching ratios of residual radioactive isotopes (RIs) resulting from OMC [5,17,18]. In this case, the experimental branching ratios of RIs after OMC are compared with the PNEM output to identify significant giant resonance (GR) peaks in the reaction.

Furthermore, the universal axial vector reductions from a single beta matrix $M(\beta^-)$ obtained from CER on ^{100}Mo have been previously published [1,7,19]. In the present study, we report, for the first time, experimental investigations of the OMC rate for ^{100}Mo, which is of interest in the context of double-β decay (DBD) and astro-antineutrinos. Additionally, we compare this rate with the OMC rate for ^{nat}Mo to analyze the dependence of the rates on A or $N - Z$. Furthermore, we

discuss a comparison with empirical rates and trends from the Goulard-Primakoff (GP) and Primakoff (P) models based on experimental OMC rates.

II. METHODOLOGY

The ^{100}Mo target is one of the candidates for supernova neutrinos and supernova antineutrinos detections [1,4,20–24]. ^{100}Mo is an interesting nucleus because of the large neutron excess $N - Z$. As the targets, a 255.1 mg cm^{-2} thick ^{100}Mo oxide powder with 96.5% enrichment and a 4.1 g cm^{-2} thick ^{nat}Mo metallic plate were utilized. The ^{nat}Mo contents 9.74% of ^{100}Mo, 24.3% of ^{98}Mo, 9.58% of ^{97}Mo, 16.7% of ^{96}Mo, 15.9% of ^{95}Mo, 9.19% of ^{94}Mo, and 14.7% of ^{92}Mo.

The experiment was carried out at Osaka University's Research Centre for Nuclear Physics (RCNP) with the use of a 0.4 kW proton beam accelerated by a ring cyclotron. Muons are generated in the MuSIC facility via proton-graphite interactions in the solenoid capture section, according to [25]. The 36° muon transport solenoid conveyed the 16 MHz continuous time structure (i.e., nonpulsed/nonbunched) muon beam to the beam outlet, where the experimental area was positioned. The 45–55 MeV c^{-1} continuous muon beam was focused on a target 5 cm away from the beam exit ($\approx 10^4$–10^5 muons/s). The ^{100}Mo target was irradiated for eight hours, with a total of 0.35×10^4 muons stopped on the target at 45 MeV c^{-1}. In contrast, ^{nat}Mo was irradiated for 6.5 hours, with an average total of 1.3×10^4 muons stopped on the target at 55 MeV c^{-1}. The probability of muons stopping in ^{100}Mo is about 99%, while in the degrader (Al) it is about 7%. Consequently, the small contribution from the degrader to the time spectrum for ^{100}Mo [Fig. 2(a)] is concealed within the background and is accounted for as part of the systematic error. The probability of muons stopping in the thick ^{nat}Mo plate is almost 100% because the degrader is not inserted.

The 3 mm thick Al degrader was applied after the S2 scintillation counter and before target in the ^{100}Mo irradiation to slow down the incoming negative muons and stop them in the targets. The expected muon momentum reaching the target is not so different due to low density of both S2 and the Al degrader, and the momentum width at MuSIC facility in 2018 is 5%. The degrader was removed during the ^{nat}Mo irradiation.

The experimental setup is illustrated in Fig. 1. When a negative muon triggers two scintillation counters (S_1 and S_2) and there are no signals from the third counter (S_3), it indicates that the muon has been stopped at the Mo target. The start time signal from S_1, S_2, and S_3 is shown in Fig. 1.

To detect outgoing gamma rays and muonic x rays, we employed one planar-type and two coaxial end-type high purity germanium (HPGe) detectors (designated as G_1, G_2, and G_3). The signals from S_1, S_2, and S_3 were recorded using three analog-to-digital converter (ADC) channels (ch0, ch1, and ch2). Nuclear gamma rays with a short lifetime of less than 1 s were recorded in channels ch3, ch4, and ch5.

For precise time measurements, we used a single-channel analyzer/time-amplitude converter (SCA/TAC) (OR-TEC 567) as a time calibrator. This allowed us to measure the time when negative muons hit S_1 and S_2, but not S_3. The time information started with the muon stopping event and ended
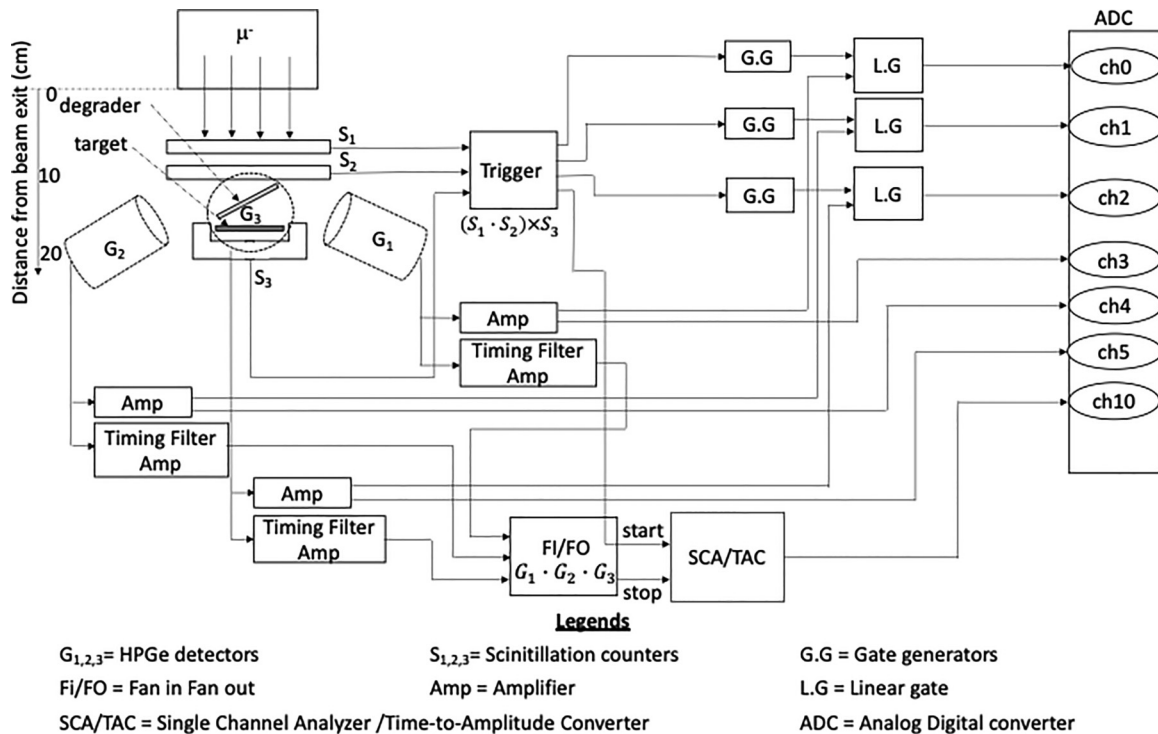
FIG. 1. Experimental setup and electronic configuration of muon irradiation on ^{nat}Mo and ^{100}Mo at RCNP, Osaka University's MuSIC facility.

when prompt nuclear gamma rays were recorded in G_1, G_2, or G_3 within a 1 µs time window. The time spectrum of these events, corresponding to the muon stopping on the target, was recorded in channel 10.

III. RESULTS AND DISCUSSION

Muons are stopped at the target and trapped in the atom's inner orbit, where they either decay into a muon neutrino and an electron or undergo muon capture on the nucleus, leading to their disappearance. The initial muon polarization, which starts at around 60%, undergoes a significant reduction through the cascade process until the muon reaches the inner bound orbit. As a consequence, there is almost no muon spin resonance (µSR) oscillation observed in the time spectra of the OMC gamma rays. Furthermore, the Ge detectors detect electrons resulting from the leptonic decay, accounting for approximately 5% of the events.

The total rate in Eq. (1), which is the inverse of the muon lifetime, was determined by observing the prompt gamma rays emitted during the OMC process. It is worth noting that the time interval between the OMC and the gamma emission is typically on the order of picoseconds or even shorter, and thus is neglected.

Figure 2 illustrates the electron time distributions for enriched ^{100}Mo and ^{nat}Mo, while the fitting results are listed in Table I. The oscillating pattern observed in the time spectra of the OMC gamma rays is considered to be due to the background oscillation of ±10 counts at around 16 MHz. This frequency corresponds to the intense protons hitting the pion

(muon) production target. Note that the background oscillations are hidden in the case of ^{100}Mo.

The muon absolute lifetimes for ^{100}Mo and ^{nat}Mo were evaluated from the observed time spectra of the electrons within a 1 µs time window from the muon stop. The measured decay curves were fitted by $N(t) = N_{BG} + N_\mu(t) \exp(-t/\tau_\mu)$, assuming that the hyperfine effect on molybdenum is very small [14]. Here, N_{BG} represents the background counts coming from the muon beam production and the transport devices. $N_\mu(t)$ represents the number of initial isotopes generated at time t, t represents the measurement time, and τ_μ represents the muon absolute lifetime.
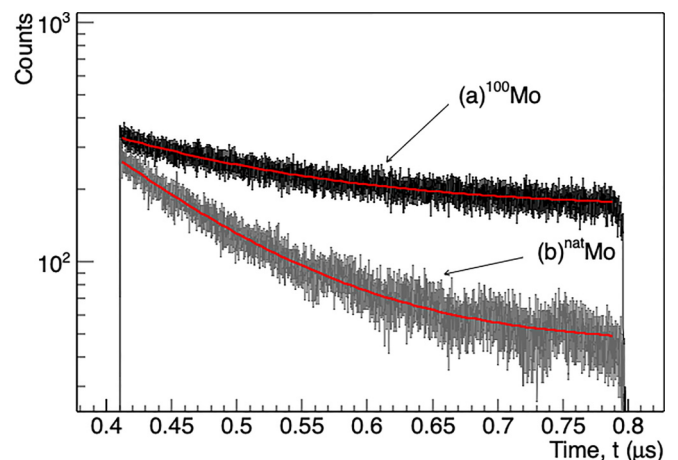

FIG. 2. Electron time distributions for (a) ^{100}Mo and (b) ^{nat}Mo.

TABLE I. Fit results of the ^{100}Mo and ^{nat}Mo (in ch10, 100 MHz TDC). Δ refers to the fitting errors, which are mainly statistical errors.

Isotope	τ_μ (ns)	$\Delta\tau_\mu$ (ns)	N_μ	ΔN_μ	N_{BG}	ΔN_{BG}
^{100}Mo	133.4	6.0	3568	142.7	170.2	6.8
^{nat}Mo	99.1	4.5	13924	542.7	43.3	0.8

Due to the short exposure period and technical disruptions of the accelerator in the initial phase of data gathering, the time distributions for ^{100}Mo and ^{nat}Mo exhibit straightforward exponential decay curves with large statistical variations throughout the measurement. The fit results in Table I include a systematic error arising from the gain shift during nonstop monitoring with low statistics. The quality of the fit is reflected on these errors.

The absolute lifetimes for muons in ^{100}Mo and ^{nat}Mo are $\tau_\mu(^{100}\text{Mo}) = 133.4 \pm 6.0$ ns and $\tau_\mu(^{nat}\text{Mo}) = 99.1 \pm 4.5$ ns. $\tau_\mu(^{100}\text{Mo})$ is greater than $\tau_\mu(^{nat}\text{Mo})$ by a factor of 1.52. The OMC rates for ^{100}Mo and ^{nat}Mo are evaluated using Eq. (1). The OMC rates for ^{nat}Mo and ^{100}Mo are derived as $(9.66 \pm 0.44) \times 10^6$ s^{-1} and $(7.07 \pm 0.32) \times 10^6$ s^{-1}, respectively, as shown in Table II.

The present value of 9.66×10^6 s^{-1} agrees with the value of 9.614×10^6 s^{-1} by [9] for ^{nat}Mo within the errors. Note that [9] uses ^{nat}Mo with a weighted mass average of $A = 96.14 \pm 1.33$. In present observations, the OMC rate for ^{100}Mo is smaller than ^{nat}Mo. The decrement of the OMC rate for different A reflects the $N - Z$ dependence.

The OMC rate by GP is given by

$$\Lambda_\mu^{GP}(A, Z) = Z_{eff}^4 G_1 \left(1 + G_2 \frac{A}{2Z} - G_3 \frac{A - 2Z}{2Z}\right) - Z_{eff}^4 G_1 G_4 \left(\frac{A - Z}{2A} + \frac{A - 2Z}{8AZ}\right) \quad (2)$$

where $G_1 = 261$, $G_2 = -0.040$, $G_3 = -0.26$, and $G_4 = 3.24$. Additionally, Primakoff's empirical formula is given by

$$\Lambda_\mu^P(A, Z) = Z_{eff}^4 X_1 \left(1 - X_2 \frac{A - Z}{2A}\right) \quad (3)$$

where $X_1 = 170$ s^{-1} and $X_2 = 3.125$. The empirical GP formula adequately reflects the OMC rate for all nuclei with specified A and Z. This formula is an extension of the P empirical formula, with a modification that accounts for the Pauli exclusion principle in medium-heavy nuclei. The recommended discrepancy between the GP and P empirical formulas for individual isotopes is set to be around 10% [21].

TABLE II. Comparison of OMC rates for Mo nuclei reported by [9] (in column 2), and the present experiment in column 3.

Isotopes	$\Lambda_\mu^{cap} \times 10^6$ s^{-1} [9]	$\Lambda_\mu^{cap} \times 10^6$ s^{-1} (this work)
^{nat}Mo	9.614 ± 0.15	9.66 ± 0.44
^{100}Mo		7.07 ± 0.32

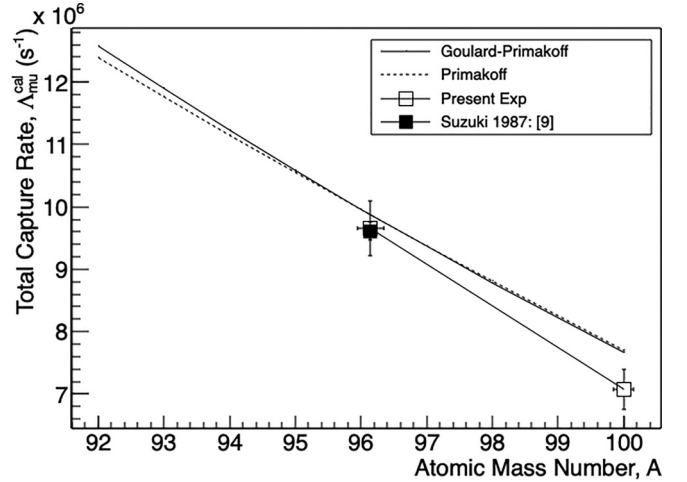

FIG. 3. Calculated and experimental OMC rates as a function of A for all Mo isotopes. The weighted average of the mass number for ^{nat}Mo is 96.14 ± 0.20. The weighted average for ^{100}Mo is 99.8 and the deviation from 100 is less than 0.15. A small difference is observed in the low A region between GP and P values.

Figure 3 illustrates the overall calculations using the GP and P empirical formulas for molybdenum isotopes with $92 \leqslant A \leqslant 100$. The present experimental data obtained from the above evaluation and the experimental data reported in [9] are included for comparison. Both empirical equations show decreasing trends for Mo isotopes as the mass number A increases. The GP and P values are slightly deflected at low A due to the inclusion of higher-order Pauli corrections for heavy elements in the GP empirical formula.

In the present work, the experimental data agree with both the GP and P empirical values. The present OMC rates for ^{nat}Mo and ^{100}Mo are within 10% errors of GP and P values, where the OMC rate for $A = 100$ is 27% lower than that for $A = 96$. The experimental rate for ^{nat}Mo from [9] yields a much lower value (around 9%) than the GP and P values. The OMC rate for present ^{nat}Mo and from [9] is very close to the GP and P empirical values. However, the current ^{100}Mo provides a greater departure from the empirical values. This finding suggests that the empirical GP and P formulations do not properly account for the isotope effect at very large $N - Z$ [9,14].

DBD nuclei of current interest are ^{76}Ge, ^{96}Zr, ^{100}Mo, ^{116}Cd, ^{130}Te, ^{136}Xe, and ^{150}Nd. All of them have the large neutron excess, $\Delta N \approx 4$–5, more than the average N of the same isotopes (same Z). Thus, their OMC rates and the τ^+ responses are considered to be much reduced due to the neutron excess. This has a substantial impact on OMC rates for DBD nuclei.

On a variety of compound and enriched nuclei, OMC rates have been measured using either electron decays or neutron decays [9,11,14]. The electron decays and the neutron decays for OMC rates have shown relatively consistent results. References [11,14] reported the present OMC rates vary from 450 to 12.6×10^6 s^{-1}, with an increment of A resulting in significantly lower OMC rates. Further analysis of Ca isotope using random phase approximation (RPA) [26] shows

that the N excess has a considerable impact on the OMC rate. In this case, the $N \approx Z$ isotopes have a consistently higher OMC rate than the neutron surplus nucleus. Similarly, neutron excess in a medium-heavy nucleus reduces β^+ and antineutrino responses by inhibiting 1^+ Gamow-Teller (GT) excitations [14,17,27]. Additional research into the $N - Z$ dependence for the strength distributions will be fascinating to better understand the neutrino nuclear responses using OMC processes.

Experimental strength distributions from OMC experiments are currently under development using PNEM for DBD nuclei and available OMC data [9,11,14,28]. This work was further used for the evaluation of the axial vector coupling constant g_A in comparison to ^{100}Mo capture strength using the proton-neutron quasiparticle random-phase approximation (pn-QRPA) in [29]. Here, the main contribution is due to the low spin states of 0^+, $1^\pm$, and $2^\pm$ with about 10% to 15% coming from higher spin states. Furthermore, the effective axial vector coupling constant of $g_A^{\text{eff}} \geqslant 1$ has been shown to reproduce well the observed rates for $^{\text{nat}}$Mo and ^{100}Mo in the standard random-phase approximation (SRPA) and the QRPA [21,27], and pn-QRPA calculations in [30]. Our OMC rates for ^{100}Mo and $^{\text{nat}}$Mo are within 5% different from the SRPA/QRPA [21,27]. The pn-QRPA by [30], which predicts well the observed OMC rate, uses the Foldy-Walecka formalism with additional theoretical frameworks to highlight the effect of nuclear structure on weak lepton-nucleus interactions. On the other hand, the pn-QRPA theoretical calculation using the Morita-Fujii formalism [29,31,32] gives much higher OMC rates.

Based on comparisons with numerous experimental data and the recent theoretical model calculations, the values for the effective axial vector coupling constant g_A^{eff} are around 0.5 [29,33] and 1.0–1.27 [21,30]. The extraction of the τ^+ responses from the muon capture strength could aid in determining the best g_A^{eff} to use in reproducing the absolute capture strength and understanding the $M^{0\nu}$.

IV. CONCLUDING REMARKS

OMC on the nucleus is a weak semileptonic process that can be used to explore neutrino nuclear responses important for DBD and astro-antineutrino nuclear responses. It can

provide information on the τ^+ responses associated with the DBD nuclear matrix element (NME) intermediate states. The τ^+ responses describe the overall final state distribution following the muon capture procedure.

The experimental OMC rates for ^{100}Mo and $^{\text{nat}}$Mo are determined by examining the time spectra of the electron decaying from the trapped muon. The OMC rate for ^{100}Mo is 27% lower than the rate for $^{\text{nat}}$Mo, with the effective A around 96 due to the blocking effect of the surplus neutrons in ^{100}Mo. The present experiment show, for the first time, a significant reduction in the OMC rate for the DBD nucleus of ^{100}Mo with $N - Z = 16$ compared to the rate for $^{\text{nat}}$Mo with $A \approx 96$ and $N - Z = 12$. This $N - Z$ dependence is consistent with the general $N - Z$ dependence observed in other nuclei [9,26] and supports the phenomenological OMC rate as a function of $N - Z$ proposed by Primakoff [34]. This demonstrates that some g_A quenching was detected in nuclear structural effects on the OMC process. Using this suggested g_A^{eff} range, the neutrino nuclear response (square of absolute NME) for DBD nuclei can, on the other hand, be calculated using the pn-QRPA theoretical calculation, which is also being done at Jyvaskyla [31,32]. The absolute and relative OMC rates as a function of excitation energy may aid theories in evaluating $0\nu\beta\beta$ NMEs and astro-antineutrino synthesis/interaction NMEs. The Ordinary Muon Capture for Double Beta Decay (OMC4DBD/MONUMENT) Collaboration is conducting extensive experimental programs on OMCs to study nuclear responses for DBD neutrinos and supernova neutrinos at the RCNP in Osaka, Japan, and the Paul Scherrer Institute (PSI) in Zurich. There is a plan for remeasuring the mass-number distribution of RIs from OMC on ^{100}Mo at PSI to check the possibility of extracting the partial OMC rates.

[1] H. Ejiri, J. Suhonen, and K. Zuber, Neutrino–nuclear responses for astro-neutrinos, single beta decays and double beta decays, Phys. Rep. **797**, 1 (2019).

[2] J. D. Vergados, H. Ejiri, and F. Šimkovic, Theory of neutrinoless double-beta decay, Rep. Prog. Phys. **75**, 106301 (2012).

[3] H. Ejiri, Experimental approaches to neutrino nuclear responses for $\beta\beta$ decays and astro-neutrinos, Front. Phys. **9**, 650421 (2021).

[4] H. Ejiri, J. Engel, and N. Kudomi, Supernova-neutrino studies with ^{100}Mo, Phys. Lett. B **530**, 27 (2002).

[5] I. H. Hashim and H. Ejiri, Ordinary muon capture for double beta decay and anti-neutrino nuclear responses, Front. Astron. Space Sci. **8**, 666383 (2021).

[6] H. Ejiri and J. Suhonen, GT neutrino–nuclear responses for double beta decays and astro neutrinos, J. Phys. G: Nucl. Part. Phys. **42**, 055201 (2015).

[7] J. H. Thies, T. Adachi, M. Dozono, H. Ejiri, D. Frekers, H. Fujita, Y. Fujita, M. Fujiwara, E.-W. Grewe, K. Hatanaka, P. Heinrichs, D. Ishikawa, N. T. Khai, A. Lennarz, H. Matsubara, H. Okamura, Y. Y. Oo, P. Puppe, T. Ruhe, K. Suda *et al.*, High-resolution ^{100}Mo(^{3}He, t)^{100}Tc charge-exchange experiment and the impact on double-β decays and neutrino charged-current reactions, Phys. Rev. C **86**, 044309 (2012).

[8] F. Cappuzzello, M. Cavallaro, C. Agodi, M. Bondì, D. Carbone, A. Cunsolo, and A. Foti, Heavy-ion double charge exchange

reactions: A tool toward $0\nu\beta\beta$ nuclear matrix elements, Eur. Phys. J. A **51**, 145 (2015).

[9] T. Suzuki, D. F. Measday, and J. P. Roalsvig, Total nuclear capture rates for negative muons, Phys. Rev. C **35**, 2212 (1987).

[10] J. C. Sens, Capture of negative muons by nuclei, Phys. Rev. **113**, 679 (1959).

[11] D. Zinatulina, V. Brudanin, V. Egorov, C. Petitjean, M. Shirchenko, J. Suhonen, and I. Yutlandov, Ordinary muon capture studies for the matrix elements in $\beta\beta$ decay, Phys. Rev. C **99**, 024327 (2019).

[12] H. Fynbo, V. Egorov, V. Brudanin, M. Chirtchenko, J. Deutsch, V. Lebedev, C. Petitjean, K. Riisager, and S. Vassiliev, The muon capture rate of ^{48}Ca, Nucl. Phys. A **724**, 493 (2003).

[13] T. Mamedov, V. Grebinnik, K. Gritsai, V. Duginov, V. Zhukov, V. Ol'shevskii, and A. Stoikov, Isotope effect in nuclear capture of negative muons in xenon, JETP Lett. **71**, 451 (2000).

[14] D. Measday, The nuclear physics of muon capture, Phys. Rep. **354**, 243 (2001).

[15] I. M. Blair, H. Muirhead, T. Woodhead, and J. N. Woulds, The effect of atomic binding on the decay rate of negative muons, Proc. Phys. Soc. **80**, 938 (1962).

[16] A. Hillairet, R. Bayes, J. F. Bueno, Y. I. Davydov, P. Depommier, W. Faszer, C. A. Gagliardi, A. Gaponenko, D. R. Gill, A. Grossheim, P. Gumplinger, M. D. Hasinoff, R. S. Henderson, J. Hu, D. D. Koetke, R. P. MacDonald, G. M. Marshall, E. L. Mathie, R. E. Mischke, K. Olchanski *et al.* (TWIST Collaboration), Precision muon decay measurements and improved constraints on the weak interaction, Phys. Rev. D **85**, 092013 (2012).

[17] I. H. Hashim, H. Ejiri, T. Shima, K. Takahisa, A. Sato, Y. Kuno, K. Ninomiya, N. Kawamura, and Y. Miyake, Muon capture reaction on ^{100}Mo to study the nuclear response for double-β decay and neutrinos of astrophysics origin, Phys. Rev. C **97**, 014617 (2018).

[18] I. Hashim, H. Ejiri, F. Othman, F. Ibrahim, F. Soberi, N. Ghani, T. Shima, A. Sato, and K. Ninomiya, Nuclear isotope production by ordinary muon capture reaction, Nucl. Instrum. Methods Phys. Res., Sect. A **963**, 163749 (2020).

[19] H. Ejiri, Nuclear spin isospin responses for low-energy neutrinos, Phys. Rep. **338**, 265 (2000).

[20] H. Ejiri, J. Engel, R. Hazama, P. Krastev, N. Kudomi, and R. G. H. Robertson, Spectroscopy of Double-Beta and Inverse-Beta Decays from ^{100}Mo for Neutrinos, Phys. Rev. Lett. **85**, 2917 (2000).

[21] F. Šimkovic, R. Dvornický, and P. Vogel, Muon capture rates: Evaluation within the quasiparticle random phase approximation, Phys. Rev. C **102**, 034301 (2020).

[22] A. S. Barabash, Possibilities of future double beta decay experiments to investigate inverted and normal ordering region of neutrino mass, Front. Phys. **6**, 160 (2019).

[23] M. P. Oliviero Cremonesi, Challenges in double beta decay, Adv. High Energy Phys. **2014**, 951432 (2014).

[24] T. Stephan, R. Trappitsch, P. Hoppe, A. M. Davis, M. J. Pellin, and O. S. Pardo, Molybdenum isotopes in presolar silicon carbide grains: Details of s-process nucleosynthesis in parent stars and implications for r- and p-processes, Astrophys. J. **877**, 101 (2019).

[25] Y. Hino, Y. Kuno, A. Sato, H. Sakamoto, Y. Matsumoto, N. Tran, I. Hashim, M. Fukuda, Y. Hayashida, T. Ogitsu, A. Yamamoto, and M. Yoshida, A highly intense DC muon source, MuSIC and muon CLFV search, Nucl. Phys. B Proc. Suppl. **253-255**, 206 (2014).

[26] E. Kolbe, K. Langanke, and K. Riisager, Muon capture on neutron-rich nuclei, Eur. Phys. J. A **11**, 39 (2001).

[27] N. T. Zinner, K. Langanke, and P. Vogel, Muon capture on nuclei: Random phase approximation evaluation versus data for $6 \leqslant Z \leqslant 94$ nuclei, Phys. Rev. C **74**, 024326 (2006).

[28] D. F. Measday and T. J. Stocki, Comparison of muon capture in light and in heavy nuclei, in *VII Latin American Symposium on Nuclear Physics and Applications, 11–16 June 2007, Cusco, Peru*, AIP Conf. Proc. No. 947 (AIP, New York, 2007), p. 253.

[29] L. Jokiniemi, J. Suhonen, H. Ejiri, and I. Hashim, Pinning down the strength function for ordinary muon capture on ^{100}Mo, Phys. Lett. B **794**, 143 (2019).

[30] M. Ciccarelli, F. Minato, and T. Naito, Theoretical study of Nb isotope productions by muon capture reaction on ^{100}Mo, Phys. Rev. C **102**, 034306 (2020).

[31] L. Jokiniemi and J. Suhonen, Comparative analysis of muon-capture and $0\nu\beta\beta$-decay matrix elements, Phys. Rev. C **102**, 024303 (2020).

[32] L. Jokiniemi, J. Suhonen, and J. Kotila, Comparative analysis of nuclear matrix elements of $0\nu\beta^+\beta^+$ decay and muon capture in ^{106}Cd, Front. Phys. **9**, 652536 (2021).

[33] L. Jokiniemi and J. Suhonen, Muon-capture strength functions in intermediate nuclei of $0\nu\beta\beta$ decays, Phys. Rev. C **100**, 014619 (2019).

[34] C. W. Kim and H. Primakoff, Theory of muon capture with initial and final nuclei treated as "elementary" particles, Phys. Rev. **140**, B566 (1965).